Journal of
Synchrotron
Radiation

ISSN 1600-5775

Received 23 October 2013
Accepted 8 May 2014

# Enhanced renal image contrast by ethanol fixation in phase-contrast X-ray computed tomography

Ryota Shirai,[a] Takuya Kunii,[a] Akio Yoneyama,[b] Takahito Ooizumi,[a]
Hiroko Maruyama,[c] Thet-Thet Lwin,[c] Kazuyuki Hyodo[d] and Tohoru Takeda[c]*

[a]Graduate School of Medical Sciences, Kitasato University, 1-15-1 Kitasato, Sagamihara-shi, Kanagawa 252-0373, Japan, [b]Central Research Laboratory, Hitachi Ltd, 2520 Akanuma, Hatoyama, Saitama 350-0395, Japan, [c]Graduate School of Medical Sciences and Allied Health Science, Kitasato University, 1-15-1 Kitasato, Sagamihara-shi, Kanagawa 252-0373, Japan, and [d]High Energy Accelerator Research Organization, 1-1 Ooho, Tsukuba-shi, Ibaraki 305-0801, Japan.
*E-mail: t.takeda@kitasato-u.ac.jp

Phase-contrast X-ray imaging using a crystal X-ray interferometer can depict the fine structures of biological objects without the use of a contrast agent. To obtain higher image contrast, fixation techniques have been examined with 100% ethanol and the commonly used 10% formalin, since ethanol causes increased density differences against background due to its physical properties and greater dehydration of soft tissue. Histological comparison was also performed. A phase-contrast X-ray system was used, fitted with a two-crystal X-ray interferometer at 35 keV X-ray energy. Fine structures, including cortex, tubules in the medulla, and the vessels of ethanol-fixed kidney could be visualized more clearly than that of formalin-fixed tissues. In the optical microscopic images, shrinkage of soft tissue and decreased luminal space were observed in ethanol-fixed kidney; and this change was significantly shown in the cortex and outer stripe of the outer medulla. The ethanol fixation technique enhances image contrast by approximately 2.7–3.2 times in the cortex and the outer stripe of the outer medulla; the effect of shrinkage and the physical effect of ethanol cause an increment of approximately 78% and 22%, respectively. Thus, the ethanol-fixation technique enables the image contrast to be enhanced in phase-contrast X-ray imaging.

**Keywords: phase-contrast X-ray CT; crystal X-ray interferometer; phase shift; ethanol-fixation; kidney.**

## 1. Introduction

Conventional X-ray imaging techniques, which are based on differences in linear attenuation coefficients, are widely used in biomedical fields. Air, soft tissue and bone can be clearly differentiated in the images. However, the differences in the linear attenuation coefficients of soft tissue are very small, so the sensitivity is too low to depict the detailed inner structures of soft tissue. Thus, in biomedical fields, iodinated contrast agents are widely used to visualize various inner structures.

Recently, a phase-contrast X-ray imaging technique for detecting contrast from differences in refractive index was developed. This technique has an approximately 1000 times greater sensitivity than that of the conventional absorption technique (Momose & Fukuda, 1995; Takeda *et al.*, 1995). The following four techniques are currently used for phase-contrast X-ray imaging: use of a Bonse–Hart type of crystal X-ray interferometer (Bonse & Hart, 1965; Becker & Bonse, 1974; Momose, 1995); crystal diffraction (diffraction enhanced imaging) (Chapman *et al.*, 1997); use of a grating interferometer (Momose *et al.*, 2003; Weitkamp *et al.*, 2005); and the propagation-based technique (Snigirev *et al.*, 1995; Wilkins *et al.*, 1996). Among these techniques, use of a Bonse–Hart type of crystal X-ray interferometer has the highest sensitivity and enables us to perform fine observations of soft tissues at 30–50 µm spatial resolution (Beckmann *et al.*, 1997; Momose *et al.*, 1996, 1998, 2000; Takeda *et al.*, 1998, 2000*a*,*b*, 2002, 2007, 2012; Noda-Saita *et al.*, 2006; Yoneyama *et al.*, 2008). In addition, to obtain images on a histological level, a micro-phase-contrast X-ray computed tomography (CT) system (Momose *et al.*, 2003) was reconstructed at SPring-8. Formalin-fixed renal structures of hamster such as the glomeruli and ductal structures were visualized at 9 µm spatial resolution (Wu *et al.*, 2009). From a biomedical point of view, a spatial resolution of 2–3 µm allows detailed histo-pathological analysis to be performed (Bentley *et al.*, 2007).

To enhance image contrast and enable higher spatial resolution to be obtained, we changed the fixation technique of a

doi:10.1107/S1600577514010558

biological sample from the commonly used formalin to ethanol. Ethanol fixation is popularly used to prepare specimens for biopsy processing and rapid intra-operative pathological diagnosis, and has been recently used to evaluate RNA and immune-staining processing due to improved immune-histological staining and the excellent yield of RNA (Cox *et al.*, 2006; Milcheva *et al.*, 2013). It exhibits comparable histology results and superior immune-staining results to formalin. We surmise that its physical properties increase the density differences against the background, and the dehydration by ethanol increases the soft tissue density. In a preliminary experiment with ethanol fixation, image contrast was significantly improved in the brain (Takeda *et al.*, 2013), heart (Kunii *et al.*, 2012, 2013) and kidney (Shirai *et al.*, 2012*a*,*b*) of a rat. Here, the quality and degree of contrast enhancement of ethanol-fixed kidney has been compared with that of the formalin-fixed kidney in phase-contrast X-ray images, and the histological changes were investigated.

## 2. Materials and methods

### 2.1. Phase-contrast X-ray CT system

The phase-contrast X-ray CT system consisted of an asymmetric Si(220) crystal forming a two-dimensional beam, a two-crystal X-ray interferometer (Yoneyama *et al.*, 2004, 2005), a phase shifter and a lens-coupling X-ray charged-coupled device (CCD) camera (Fig. 1). The interferometer consists of two crystal blocks having two crystal wafers. The incident X-ray beam was divided into two coherent beams by the first wafer (S: splitter) of the first crystal block using Laue-case X-ray diffraction. These two beams were reflected by the second wafer ($M_1$: mirror) of the first crystal block and the first wafer ($M_2$: mirror) of the second crystal block, respectively, and recombined at the second wafer (A: analyzer) of the second crystal block to create two interference beams. The phase shift caused by the samples set in one beam path of the interferometer can be detected by the change of the beam intensity of the interference beams.

The X-ray imager consists of a scintillator ($Gd_2O_2S$) that converts X-rays into visible light, and a relay-lens system that transfers the light from the scintillator to a CCD camera. The field of view of the detector is 16 mm × 13 mm. It is composed of 1300 × 1000 pixels, with each pixel being 13 µm × 13 µm (in the 2 × 2 binning mode).

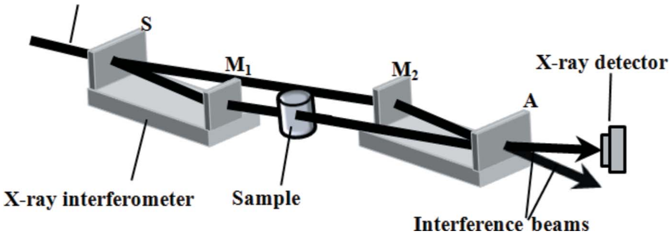

**Figure 1**
Phase-contrast X-ray CT system with two-crystal X-ray interferometer.

The experiment was performed at the vertical wiggler beamline BL14C of the Photon Factory, High Energy Accelerator Research Organization (KEK), Tsukuba, Japan. The X-ray energy was set to 35 keV by the monochromator, and the X-ray flux in front of the sample cell was approximately $4.0 \times 10^7$ counts $s^{-1}$ $mm^{-2}$ at a ring current of 450 mA with 2.5 GeV storage energy.

### 2.2. Animal preparation

This study used six male rats (age: 10 weeks; weight: ∼300 g each). All rats were anesthetized, and cannulation to the apex of the left ventricle was carried out surgically for perfusion. First, physiological saline solution was injected from the apex, and the blood in the vessel was replaced to eliminate blood coagulation artefacts. Then, 10% formalin or 100% ethanol was perfused for fixation, and the samples were steeped in each fixing solution.

This experiment was approved by the Medical Committee for the Use of Animals in Research of Kitasato University, and conformed to the guidelines of the American Physiological Society.

### 2.3. Image data acquisition

For phase-contrast X-ray imaging, the specimen was placed in a 15 mm-thick cell filled with formalin for formalin-fixed kidney or ethanol for ethanol-fixed kidney. The cells were inserted into the beam path between $M_1$ and A of the X-ray interferometer, as shown in Fig. 1.

A phase map was obtained by fringe-scan method with three images changing by $2\pi/3$. The beam exposure time was 10 s per projection and the total number of projections was 250 over 180°. The CT image was reconstructed by a filtered back-projection method.

### 2.4. Histological staining

After phase-contrast X-ray CT imaging, all specimens fixed by each solution (ethanol and formalin) were sliced into 3 µm-thick sections and stained with hematoxylin and eosin (HE). Histological images were assessed using an optical microscope equipped with a camera (DP21; OLYMPUS, Japan).

Here, the mechanism of the fixation technique must be recognized for quantitative analysis of histological images. Formalin causes the insolubility of tissue by polymerizing the intermolecular methylene bridge between the protein and peptide. Ethanol is used in the HE staining process. Thus, shrinkage of tissue by this process must be considered when evaluating histological structures. However, shrinkage of the formalin-fixed tissue by this process is reported to be very small because the mesh of the methylene bridge holds the tissue structure (Baker, 1958; Boon & Drijver, 1986; Horobin, 1982).

### 2.5. Image analysis

In the quantitative analysis of phase-contrast X-ray images, the density calculated by refraction index was determined directly from phase shift information (Yoneyama *et al.*, 2011).

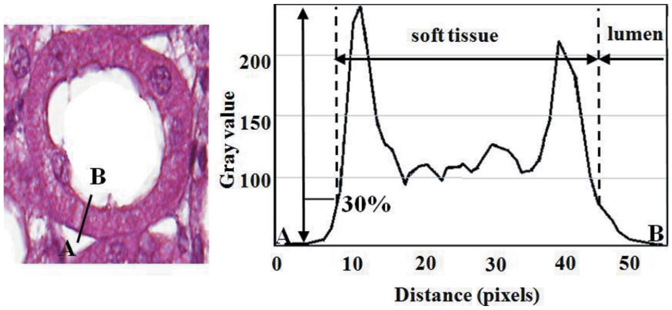

**Figure 2**
Decision of the percentage soft tissue area per unit. The margin between lumen and soft tissue is decided by a 30% cut-off level.

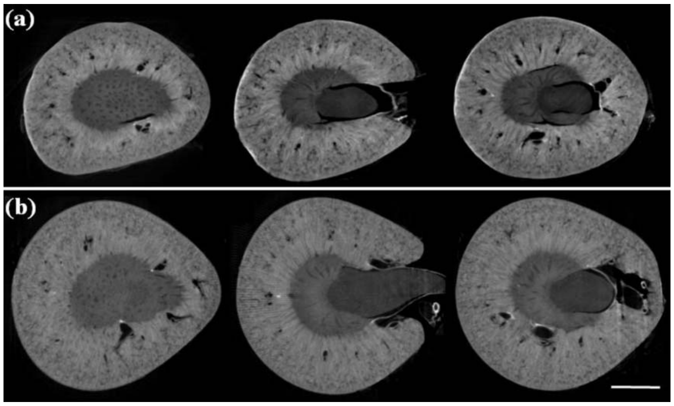

**Figure 3**
Images obtained by phase-contrast X-ray CT of kidney at 35 keV. The image was standardized at a 512 grey level. (*a*) Ethanol-fixed. (*b*) Formalin-fixed. Scale bar: 1 mm.

Measurement in the phase-contrast X-ray CT images was performed at each of 12 regions of interest in the cortex, outer stripe of the outer medulla (OS), inner stripe of the outer medulla (IS), inner medulla (IM) and renal pelvis (RP).

In histological analysis, to evaluate the change of density by fixation techniques in a phase-contrast X-ray image, an optical microscopic image was analyzed quantitatively. To determine the percent soft tissue area per unit, a cut-off level of 30% was chosen for distinguishing between lumens and soft tissue in the histological images of cortex and OS (Fig. 2). Quantitative image analysis was performed by using image-manipulating software (*NIH Image* version 1.63, http://rsb.info.nih.gov/nih-image).

All values are expressed as means ± standard deviation. Statistical differences between groups are evaluated using an unpaired Student's t-test. A $p$ value of less than 0.05 is considered to indicate a statistically significant difference.

**2.5.1. Quantification of density in phase-contrast X-ray image**. The refraction index was determined directly from the phase-shift information. The mass density $\rho$ was calculated using the following equations,

$$\delta = \Delta p \lambda / 2 \pi t, \qquad \rho = 4 \pi \delta / \lambda^2 r_e N_A,$$

where $\Delta p$ is the phase value, $\delta$ is the real part of the refractive index, $t$ is the pixel size, $\lambda$ is the X-ray wavelength, $r_e$ is the classical electron radius and $N_A$ is Avogadro's number.

## 3. Results

### 3.1. Phase-contrast image

Phase-contrast X-ray CT revealed the structures of the renal cortex, medulla and vessels in both formalin- and ethanol-fixed kidneys (Fig. 3); however, the image contrast of ethanol-fixed tissues was much better than that of formalin-fixed tissues. The renal structure was divided into the following five regions: cortex, OS, IS, IM and RP. These divisions were used both in phase-contrast X-ray CT images and in optical microscopic images (Fig. 4).

In phase-contrast X-ray CT images, the absolute density with ethanol fixation was 0.854 ± 0.011 g cm$^{-3}$ in the cortex, 0.869 ± 0.012 g cm$^{-3}$ in the outer stripe of the outer medulla, and 0.826 ± 0.001 g cm$^{-3}$ in the renal pelvis (Fig. 5*a*), respectively; that with formalin fixation was 1.040 ± 0.014 g cm$^{-3}$ in the cortex, 1.043 ± 0.010 g cm$^{-3}$ in the outer stripe of the outer medulla, and 1.025 ± 0.010 g cm$^{-3}$ in the renal pelvis (Fig. 5*b*).

The percent image contrast against background solution in the phase-contrast X-ray CT image with ethanol fixation was 8.3% in the cortex, 10.1% in the outer stripe of the outer medulla, 6.5% in the inner stripe of the outer medulla, 5.4% in the inner medulla and 4.7% in the renal pelvis; that with formalin fixation was 3.0% in the cortex, 3.2% in the outer stripe of the outer medulla, 2.0% in the inner stripe of the outer medulla, 1.7% in the inner medulla and 1.5% in the renal pelvis (Fig. 5*c*). Therefore, the image contrast of ethanol-fixed tissue was approximately three times higher than that of formalin-fixed tissue.

The absolute density difference between tissue and background with ethanol fixation was 65.3 ± 2.1 mg cm$^{-3}$ in the

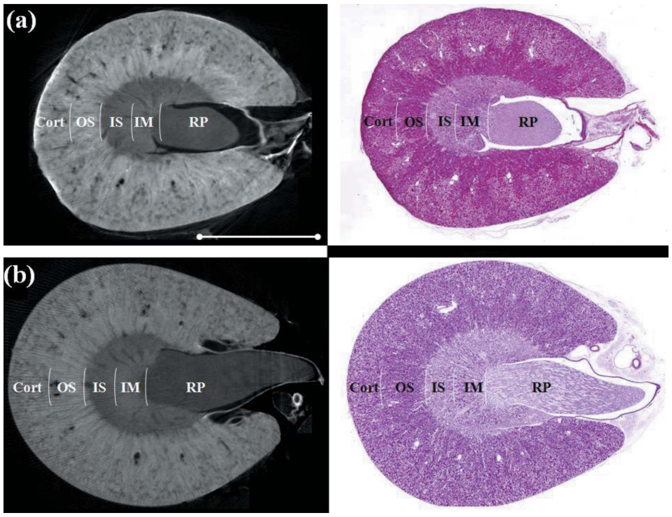

**Figure 4**
Phase-contrast X-ray CT image and histological image stained with hematoxylin and eosin. The renal cortex (Cort), outer stripe of the outer medulla (OS), inner stripe of the outer medulla (IS), inner medulla (IM) and renal pelvis (RP) are clearly distinguished. Scale bar: 2.5 mm.

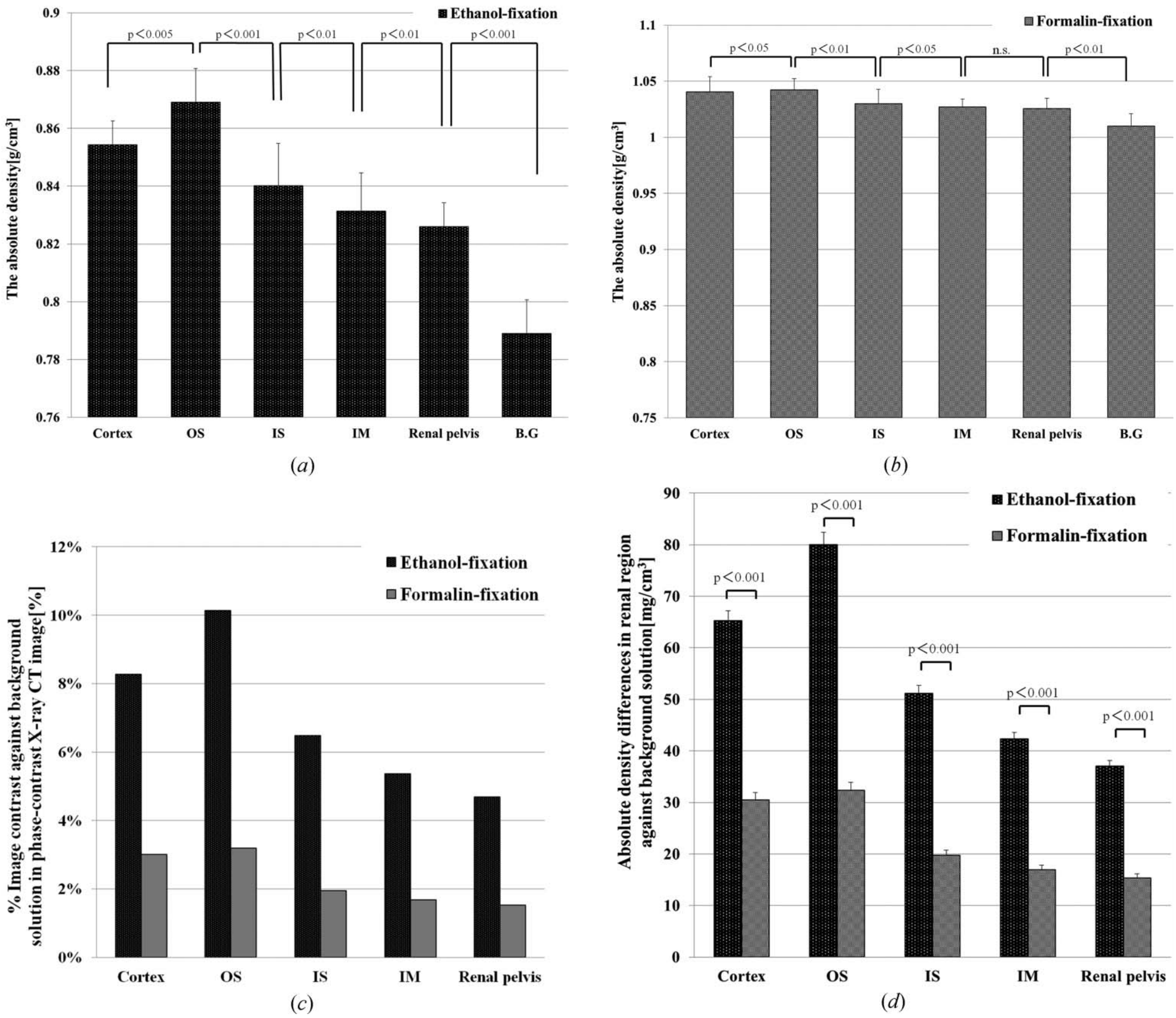

**Figure 5**

Absolute density obtained from phase-contrast X-ray CT. (*a*) Ethanol fixation. (*b*) Formalin fixation. (*c*) Percent image contrast against background solution in the phase-contrast X-ray CT image. (*d*) Absolute density difference in the renal region against background solution.

cortex, 80.0 ± 2.5 mg cm$^{-3}$ in the outer stripe of the outer medulla, and 37.0 ± 1.6 mg cm$^{-3}$ in the renal pelvis; that with formalin fixation was 30.4 ± 2.0 mg cm$^{-3}$ in the cortex, 32.3 ± 2.3 mg cm$^{-3}$ in the outer stripe of the outer medulla, and 15.4 ± 1.4 mg cm$^{-3}$ in the renal pelvis (Fig. 5*d*).

### 3.2. Optical microscopic image

In the optical microscopic images, the inner renal structures were visualized well, and the contraction of soft tissue and decreased luminal space were observed markedly in ethanol-fixed kidney (Fig. 6). This change was significantly observed in the cortex and OS, particularly in the OS.

In quantitative histological analysis, the area ratios of soft tissue against lumens of the renal tubules and vessels fixed by ethanol were 68.9 ± 3.4% in the cortex, 68.4 ± 4.0% in OS, 54.4 ± 2.1% in IS, 51.1 ± 2.5% in IM and 38.0 ± 2.3% in RP. On the other hand, the area ratios for formalin-fixed tissues were 52.1 ± 3.8% in the cortex, 49.1 ± 3.3% in OS, 42.6 ± 3.7% in IS, 40.5 ± 2.0% in IM and 30.9 ± 1.9% in RP (Fig. 7).

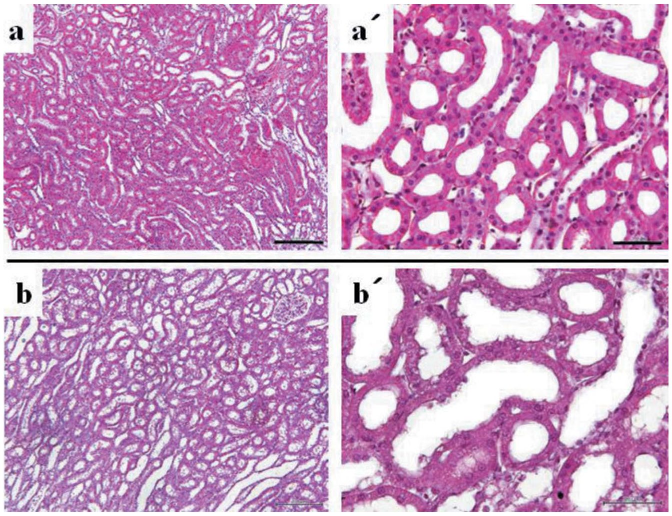

**Figure 6**

Histological image of kidney stained with hematoxylin and eosin. (*a*) Ethanol-fixed outer stripe of the outer medulla (OS). (*b*) Ethanol-fixed inner stripe of the outer medulla (IS). Scale bar: 100 µm. (*a*′) Ethanol-fixed outer stripe of the outer medulla (OS). (*b*′) Formalin-fixed outer stripe of the outer medulla (OS). Scale bar: 25 µm.

**Table 1**
Absolute density estimation from the histological image, and the density obtained by phase-contrast X-ray CT.

The density in RP was assumed to be the absolute density of fluid, both intra- and extra-fluid, due to the mixed ethanol or formalin. Then, the absolute soft tissue density including the protein and nucleic acid as DNA and RNA is 28.2 mg cm$^{-3}$ in the cortex, 43.0 mg cm$^{-3}$ in OS, 14.1 mg cm$^{-3}$ in IS and 5.3 mg cm$^{-3}$ in IM for ethanol. On the other hand, it is 15.1 mg cm$^{-3}$ in the cortex, 16.9 mg cm$^{-3}$ in OS, 4.4 mg cm$^{-3}$ in IS and 1.6 mg cm$^{-3}$ in IM for formalin. Therefore, the increased density by renal tissue shrinkage is calculated as 27.5 mg cm$^{-3}$ in the cortex, 41.5 mg cm$^{-3}$ in OS, 6.5 mg cm$^{-3}$ in IS and 2.1 mg cm$^{-3}$ in IM. In the cortex and OS, the estimated absolute density is almost the measured density by phase-contrast X-ray CT (PCCT).

| | Cortex | Outer stripe of outer medulla | Inner stripe of outer medulla | Inner medulla |
|---|---|---|---|---|
| % Soft tissue area by ethanol ($A$) | 68.9 | 68.4 | 54.4 | 51.1 |
| % Soft tissue area by formalin ($B$) | 52.1 | 49.1 | 42.6 | 40.5 |
| Area ratio of $A$/$B$ | 32.1 | 39.2 | 27.8 | 26.2 |
| Volume ratio of $A$/$B$ | 181.9 | 245.4 | 146.6 | 134.1 |
| Absolute tissue density of $B$ (PCCT) | 15.1 | 16.9 | 4.4 | 1.6 |
| Estimated absolute density | 27.5 | 41.5 | 6.5 | 2.1 |
| Absolute tissue density of $A$ (PCCT) | 28.2 | 43 | 14.1 | 5.3 |

## 4. Discussion

The aim of ethanol fixation is considered in two points: the first is physically to enhance the density difference between the soft tissue and surrounded ethanol solution with lower density (0.79 g cm$^{-3}$) than that of formalin solution (1.01 g cm$^{-3}$), and the second is histologically shrinkage/dehydration due to ethanol. These effects of ethanol enable excellent image contrast to be obtained compared with that of formalin-fixed kidney in phase-contrast X-ray images and absorption-contrast X-ray images. Actually, in phase-contrast X-ray CT, the percentage image contrast by ethanol was approximately three times higher than that by formalin in all regions, as shown in Fig. 5(*c*). The absolute density difference of ethanol fixation against formalin fixation also increased in all regions, as shown in Fig. 5(*d*) and Table 1. However, the absolute density could be evaluated exactly in the cortex and OS, so these regions were used for quantitative analysis. The percent image contrast generated by physical effects and increased tissue density is approximately 2.7 times in the cortex and 3.2 times in OS, whereas the increased absolute density was approximately 2.1 times in the cortex and 2.5 times in OS. Thus, dividing the percent image contrast by the increased absolute density resulted in values of approximately 1.3. Then, in phase-contrast X-ray imaging with ethanol fixation, the image contrast was approximately three times higher than that with formalin fixation, with approximately 78% shrinkage of tissue and 22% physical effect by ethanol.

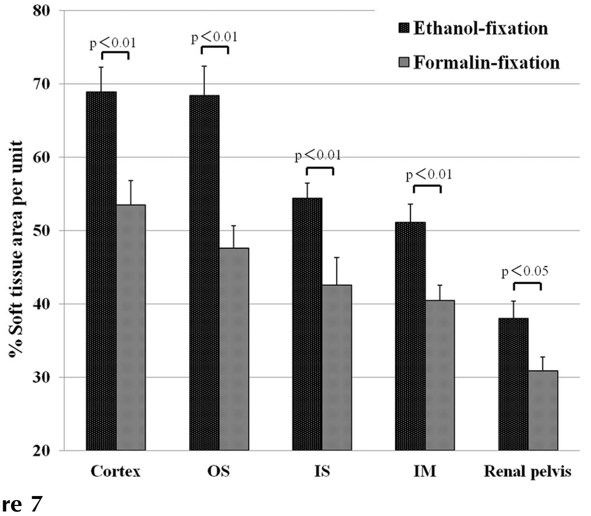

**Figure 7**
Percent soft tissue area per unit obtained from optical microscopic images.

In the optical microscopic images, regions of the renal cortex and OS shown with high density by phase-contrast X-ray CT imaging had thicker tubular wall and narrower luminal space than other renal regions, as shown in Fig. 6. After ethanol fixation, quantitative histological analysis showed that the percentile soft tissue area against lumens was significantly increased. The increased ratios of the soft tissue areas in ethanol-fixed tissues compared with formalin-fixed tissues were 32.1% in the cortex, 39.2% in OS, 27.8% in IS, 26.2% in IM and 23.1% in RP (Table 1). Here, the percent increased soft tissue by shrinkage in voxel-base can be estimated as shown in Table 1. From these values, absolute density changes could be estimated theoretically. In the cortex and OS, the estimated absolute density is almost the measured density by phase-contrast X-ray CT imaging. In the regions of IM and IS, the absolute density is significantly lower than that of phase-contrast X-ray CT, probably due to an inadequate cut-off level decision. In these regions, the tubular wall is very thin, so the cut-off level should be set to a much lower value. From these results, the shrinkage of formalin-fixed samples by pre-processing of HE staining is not as significant a problem as previous reported (Baker, 1958; Boon & Drijver, 1986; Horobin, 1982).

Using this ethanol-fixation technique, the image contrast of phase X-ray imaging has been enhanced approximately three times. This increased image contrast improves the spatial resolution due to an increased signal-to-noise ratio per area, and enables biological specimens resembling the histological image to be observed. In micro-absorption CT with osmium enhancement, it is reported that various renal structures such as glomeruli, nephrons and their lumens were well demonstrated at 2 μm spatial resolution; however, only large ducts and glomeruli could be visualized at 6 μm spatial resolution (Bentley *et al.*, 2007). For the micro-phase-contrast X-ray image obtained at SPring-8, glomeruri and ductal structures were well visualized without contrast enhancement (Wu *et al.*, 2009); however, the spatial resolution is insufficient as mentioned above. By increasing the X-ray flux density, higher spatial resolution can be obtained. However, high X-ray flux causes damage to biological specimens in the form of shrinkage; actually, about 2.5% shrinkage occurred in the phase-contrast X-ray image obtained at SPring-8 (about 1000 times higher X-ray flux than at KEK). We would therefore like to obtain images at lower X-ray dose. Without the use of a heavy metal, phase-contrast X-ray CT imaging with 2–3 µm spatial resolution is thought to be suitable for detailed histological investigations.

The present study has some limitations in visualizing the image with high spatial resolution because the phase-contrast X-ray CT system at KEK was constructed to observe large objects at spatial resolutions of 30–50 µm. In particular, each glomerulus could not be visualized well because of the limited spatial resolution of the present X-ray CCD camera system and X-ray interferometer. We are currently planning to use a new X-ray CCD camera with a spatial resolution of 3 µm, and to thin the crystal wafers of the interferometer to reduce the Borrmann fan phenomenon (Hirano & Momose, 1998) in order to obtain a system with much higher spatial resolution of 3 µm.

## 5. Conclusion

Phase-contrast X-ray imaging using a two-crystal X-ray interferometer was able to clearly detect the fine renal structures such as the cortex, medulla and vessels at 35 keV X-ray energy. The image contrast of ethanol-fixed kidneys was much better than that of formalin-fixed kidneys.

This research was supported by a grant from Kitasato University School of Allied Health Sciences (Grant-in-Aid for Research Project, Nos. 2010-1002, 2011-1009, 2012-1012), and was approved by the High Energy Accelerator Research Organization (proposal Nos. 2009S2-006, 2012-G044 and 2013-G584). We would like to thank Professor M. Minami and Mr K. Kobayashi of the University of Tsukuba for use of the phase-contrast X-ray CT system and preparing the experimental cells

## References

Baker, J. R. (1958). *Principles of Biological Microtechnique – a Study of Fixation and Dyeing.* London: Methuen.

Becker, P. & Bonse, U. (1974). *J. Appl. Cryst.* **7**, 593–598.

Beckmann, F., Bonse, U., Busch, F. & Gunnewig, O. (1997). *J. Comput. Assist. Tomogr.* **21**, 539–553.

Bentley, M. D., Jorgensen, S. M., Lerman, L. O., Ritman, E. L. & Romero, J. C. (2007). *Anat. Rec.* **290**, 277–283.

Bonse, U. & Hart, M. (1965). *Appl. Phys. Lett.* **6**, 155–156.

Boon, M. E. & Drijver, J. S. (1986). *J. Pathol.* **151**, 168–169.

Chapman, D., Thomlinson, W., Johnston, R. E., Washburn, D., Pisano, E., Gmür, N., Zhong, Z., Menk, R., Arfelli, F. & Sayers, D. (1997). *Phys. Med. Biol.* **42**, 2015–2025..

Cox, M. L., Schray, C. L., Luster, C. N., Stewart, Z. S., Korytko, P. J., M. Khan, K. N., Paulauskis, J. D. & Dunstan, R. W. (2006). *Exp. Mol. Pathol.* **80**, 183–191.

Hirano, K. & Momose, A. (1998). *J. Synchrotron Rad.* **5**, 967–968.

Horobin, R. W. (1982). *Histochemistry. An Explanatory Outline of Histochemistry and Biophysical Staining.* London/Stuttgart: Butterworths/Fischer.

Kunii, T., Shirai, R., Yoneyama, A., Maruyama, H., Thet-Thet-Lwin & Takeda, T. (2013). *Med. Imag. Technol.* **31**, 132–135.

Kunii, T., Shirai, R., Yoneyama, A., Ooizumi, T., Maruyama, H., Thet-Thet-Lwin, Hyodo, K. & Takeda, T. (2012). *Proceedings of the BMES Annual Meeting 2012*, 1008: pp. 1–4, 24–27 October 2012, Atlanta, Georgia, USA.

Milcheva, R., Janega, P., Celec, P., Russev, R. & Babál, P. (2013). *Acta Histochem.* **115**, 279–289.

Momose, A. (1995). *Nucl. Instrum. Methods Phys. Res. A*, **352**, 622–628.

Momose, A. & Fukuda, J. (1995). *Med. Phys.* **22**, 375–379.

Momose, A., Koyama, I., Hamaishi, Y., Yoshikawa, H., Takeda, T., Wu, J., Itai, Y., Takai, K., Uesugi, K. & Suzuki, Y. (2003). *J. Phys.* **104**, 599–602.

Momose, A., Takeda, T. & Itai, Y. (2000). *Radiology*, **217**, 593–596.

Momose, A., Takeda, T., Itai, Y. & Hirano, K. (1996). *Nat. Med.* **2**, 473–475.

Momose, A., Takeda, T., Itai, Y., Yoneyama, A. & Hirano, K. (1998). *J. Synchrotron Rad.* **5**, 309–314.

Noda-Saita, K., Yoneyama, A., Shitaka, Y., Hirai, Y., Terai, K., Wu, J., Takeda, T., Hyodo, K., Osakabe, N., Yamaguchi, T. & Okada, M. (2006). *Neuroscience*, **138**, 1205–1213.

Shirai, R., Kunii, T., Yoneyama, A., Maruyama, H., Thet-Thet-Lwin & Takeda, T. (2012*b*). *Med. Imag. Technol.* **30**, 298–302.

Shirai, R., Kunii, T., Yoneyama, A., Thet-Thet-Lwin, Hyodo, K. & Takeda, T. (2012*a*). *Proceedings of the BMES Annual Meeting 2012*, 1007: pp. 1–4, 24–27 October 2012, Atlanta, Georgia, USA.

Snigirev, A., Snigireva, I., Kohn, V., Kuznetsov, S. & Schelokov, I. (1995). *Rev. Sci. Instrum.* **66**, 5486–5492.

Takeda, T., Momose, A., Hirano, K., Haraoka, S., Watanabe, T. & Itai, Y. (2000*a*). *Radiology*, **214**, 298–301.

Takeda, T., Momose, A., Itai, Y., Wu, J. & Hirano, K. (1995). *Acad. Radiol.* **2**, 799–803.

Takeda, T., Momose, A., Ueno, E. & Itai, Y. (1998). *J. Synchrotron Rad.* **5**, 1133–1135.

Takeda, T., Momose, A., Wu, J., Yu, Q., Zeniya, T., Thet-Thet-Lwin, Yoneyama, A. & Itai, Y. (2002). *Circulation*, **105**, 1708–1712.

Takeda, T., Momose, A., Yu, Q., Wu, J., Hirano, K. & Itai, Y. (2000*b*). *J. Synchrotron Rad.* **7**, 280–282.

Takeda, T., Thet-Thet-Lwin, Kunii, T., Shirai, R., Ooizumi, T., Maruyama, H., Hyodo, K., Yoneyama, A. & Ueda, K. (2013). *J. Phys.* **425**, 1–4.

Takeda, T., Wu, J., Thet-Thet-Lwin, Yoneyama, A., Hyodo, K., Matsuda, Y. & Kose, K. (2007). *J. Comput. Assist. Tomogr.* **31**, 214–217.

Takeda, T., Yoneyama, A., Wu, J., Thet-Thet-Lwin, Momose, A. & Hyodo, K. (2012). *J. Synchrotron Rad.* **19**, 252–256.

Weitkamp, T., Diaz, A., David, C., Pfeiffer, F., Stampanoni, M., Cloetens, P. & Ziegler, E. (2005). *Opt. Express*, **13**, 6296–6304.

Wilkins, S. W., Gureyev, T. E., Gao, D., Pogany, A. & Stevenson, A. W. (1996). *Nature (London)*, **384**, 335–338.

Wu, J., Takeda, T., Thet-Thet-Lwin, Momose, A., Sunaguchi, N., Fukami, T., Yuasa, T. & Akatsuka, T. (2009). *Kidney Intl*, **75**, 945–951.

Yoneyama, A., Takeda, T., Tsuchiya, Y., Wu, J., Thet-Thet-Lwin, Hyodo, K. & Hirai, Y. (2005). *J. Synchrotron Rad.* **12**, 534–536.

Yoneyama, A., Takeda, T., Tsuchiya, Y., Wu, J., Thet-Thet-Lwin, Koizumi, A., Hyodo, K. & Itai, Y. (2004). *Nucl. Instrum. Methods Phys. Res. A*, **523**, 217–222.

Yoneyama, A., Wu, J., Hyodo, K. & Takeda, T. (2008). *Med. Phys.* **35**, 4724–4734.

Yoneyama, A., Yamada, S. & Takeda, T. (2011). *InTech*, **2**, 107–128.